L- and M-shell electron shake-off accompanying alpha decay*

M. S. Rapaport, F. Asaro, and I. Perlman†
Nuclear Chemistry Division, Lawrence Berkeley Laboratory, University of California, Berkeley, California 94720
(Received 4 November 1974)

The L_{I}-, L_{II}-, L_{III}-, and M-shell vacancy distributions accompanying electron shake-off in the α decay of ^{210}Po have been measured by α-x-ray two parameter coincidence techniques. The ionization probabilities and the errors due to our measurements were $(5.11\pm0.40,\ 0.62\pm0.06,$ and $1.50\pm0.19)\times10^{-4}$ for the L_{I}, L_{II}, and L_{III} subshells, respectively, and $(1.8\pm0.4)\times10^{-2}$ for the M shell. Possible errors in tabulated fluorescence and Coster-Kronig yields could increase the uncertainties to $(1.7,\ 0.5,\ 0.8)\times10^{-4}$ and 0.6×10^{-2}, respectively. The energies and peak shapes of the α groups in coincidence with $L\alpha$, $L\beta$, $L\gamma$, and M x rays were also measured. The coincident groups were, respectively, 12.6 ± 1.4, 13.8 ± 1.4, 17.6 ± 2.1, and 3.1 ± 1.0 keV lower in energy than the ^{210}Po α_0 peak. Theoretical calculations by Hansen are in closer agreement with the experimental values for the L subshells than Migdal's theory, but discrepancies of about a factor of 2 still exist.

[RADIOACTIVITY ^{210}Po; measured α-L and α-M x-ray coin. Deduced L_{I}, L_{II}, L_{III}, M electron shake-off abundances, energy distribution.]

I. INTRODUCTION

In the preceding paper[1] we reported experimental and theoretical results on K-shell ionization (shake-off) in the α decay of ^{210}Po and ^{238}Pu. The present work was undertaken to measure the shake-off phenomenon accompanying the α decay of ^{210}Po in the L and M shells.

Several measurements of the total shake-off phenomenon in the L and M shells exist. Curie and Joliot[2] were the first to observe the soft radiation associated with α decay of ^{210}Po. They detected the photons by means of an ionization chamber connected to an electroscope and identified photon energies by absorption coefficients. They believed the radiation to be Po x rays excited by α particles. However, they stated that their technique could not distinguish between lead and polonium photons.

Riou[3] identified the L x rays associated with ^{210}Po α decay as lead x rays. He used a Geiger-Müller detector and identified the soft radiation by selective absorption coefficients. Rubinson and Bernstein[4] and later Rubinson[5] studied the L and M x rays, respectively. They used a proportional counter and were able to observe some of the structure associated with filling the vacancies in the L and M shells.

In the present work with high resolution solid state detectors the initial L-subshell vacancies and the yield of M x rays that result from the α decay of ^{210}Po were determined. In addition, that part of the α spectrum connected with the electron shake-off effect in the L and M shells was measured directly and compared with current theories. Also the differential shape of the α spectrum connected with the electron shake-off phenomenon in the L and M shells was determined.

II. EXPERIMENTAL WORK

A. Equipment

The general experimental procedure was to measure the energy and abundance of the α spectrum which was in coincidence with L and M x rays as well as the energies and abundances of the x rays.

1. Vacuum chamber

The x-ray detector housing was positioned at about the center of a cubic aluminum vacuum chamber. The housing had a 25 μm thick beryllium window which could be opened once a good vacuum was established in the chamber. A motor driven α detector penetrated the vacuum chamber from the side opposite the x-ray detector. The sources to be studied were mounted on the α detector housing about 1 cm away from the α crystal and could be brought within 3 mm of the face of the x-ray crystal. The source-to-detector distance was variable for the x-ray side but not for the α side. When a coincidence experiment was not in progress, a magnetically-controlled nickel foil could be placed between the source and the α detector to protect the latter from the intense α radiation.

A cryogenic pump, two 8 liter ion pumps and a cold finger were used to evacuate the vacuum chamber. On the average, 6 h of pumping were

needed before a pressure of $\sim 10^{-7}$ Torr was reached and the beryllium window on the face of the x-ray detector housing could be opened.

2. X-ray side

The x rays were detected with a Si(Li) solid state detector which was 5 mm in diameter and 3 mm thick. The detector had a full width at half-maximum (FWHM) of 180 eV for 6.46 keV iron $K\alpha$ x rays. In our experimental arrangement, the maximum over-all detection efficiency (which includes the geometry of the system) was 6.0% for 10 keV radiation, and at 3.3 keV this was reduced to 2.55%

To determine these efficiencies, ^{241}Am, ^{57}Co, ^{65}Zn, and ^{54}Mn were separately vaporized in vacuum from tungsten filaments onto 25 μm thick beryllium disks. The sources were collimated to an area 2 mm in diameter during vaporization. The absolute disintegration rates of the sources were determined by measuring the abundances of their γ rays and comparing them with known standards of the same isotopes. Tabulated values[6-8] of the intensities of x rays and low energy γ rays associated with the above sources were then used to determine the x-ray detector efficiency curve.

The preamplifier utilized a low-noise field-effect transistor at low temperature with pulsed optical feedback. Final amplification was accomplished by an Amplifier System Module[9] which contained a linear amplifier (17 μsec time constant), a biased amplifier, and a pileup rejector. The output was fed both into a coincidence circuit and into an analog-to-digital converter (ADC) which fed a two parameter coincidence system. The block diagram for the system is shown in Fig. 1. The linearity of the amplifier-analyzer system for x rays was better than 0.3% and no shift in energy was observed during the five months of experiments.

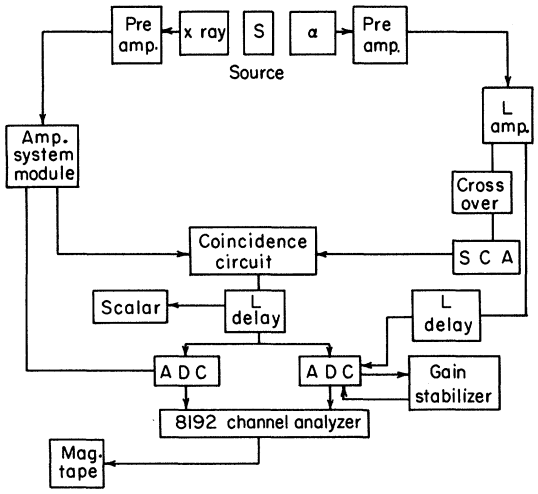

FIG. 1. Block diagram of electronic system.

3. α side

The α particles were detected with a Au-Si surface-barrier type crystal with a geometry of 0.80% and resolution of 20.0 keV (FWHM). The α detector was operated at 4°C, and no deterioration of its resolution was observed during the experiments although the pulse amplitude gradually decreased with time. The energy linearity of the amplifier-analyzer system for α particles was better than 0.5% in the region of interest.

The α detector output was amplified and then fed both into the coincidence circuit and into a separate ADC. The output from this ADC was fed into a gain stabilizer, which operated only on those α pulses that were in coincidence with x-ray pulses. After eight days of operation the gain stabilizer was not able to compensate for the decreasing preamplifier output and the pulse-height out of the amplifier also began gradually decreasing. The pulses from both the x-ray side and α side ADC's were routed into a two parameter coincidence system as shown in Fig. 1. The data were reduced with the computer program MULTI.[10]

B. Source preparation

The ^{210}Po was purchased from New England Nuclear where it was prepared by the reaction and decay:

$$^{209}\mathrm{Bi}(n,\gamma)^{210}\mathrm{Bi}\xrightarrow[5\ \mathrm{day}]{\beta-}{}^{210}\mathrm{Po}\ .$$

In addition to the ^{210}Po 803 keV γ ray, low intensity Ba K x rays were observed as well as the ^{210}Pb 47 keV γ ray. Since the above radiations do not interfere with the experiments, the ^{210}Po was not further purified.

The ^{210}Po activity was vaporized in vacuum from a tungsten filament onto a 25 μm thick beryllium disk in exactly the same way as in the efficiency determinations. The latter was thick enough to stop any of the α particles from reaching the x-ray detector. The source, which had been collimated to an area 2 mm in diameter during vaporization, had an activity of $\sim 2.6\times 10^6$ α dis/min.

C. Results

The ^{210}Po source was measured in the coincidence unit for a total of 13.3 days during the 14

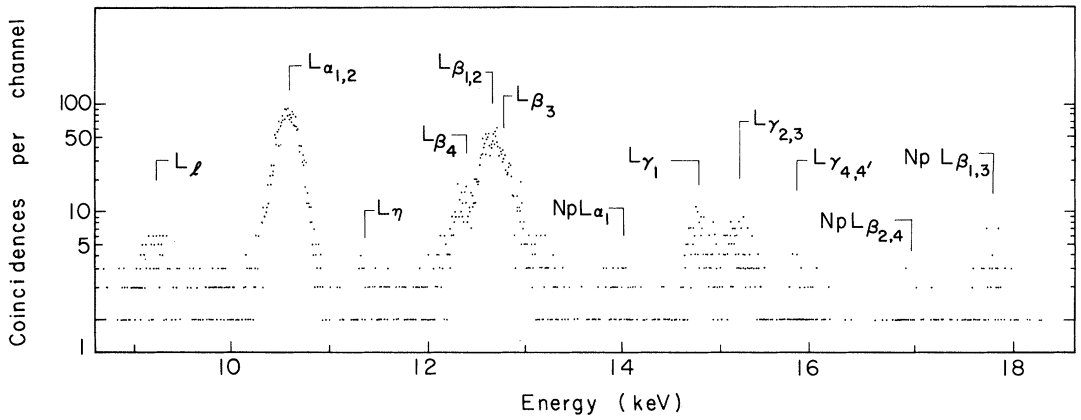

FIG. 2. Pb L x-ray spectrum (8.37 eV per channel) in coincidence with α particles.

day experiment. The α singles spectra were measured and recorded on magnetic tape every day as were the coincidence spectra. The spectrum of L x rays in coincidence with α particles is shown in Fig. 2. In Fig. 3 are shown the coincident M x rays for the same measurement. A 2.9 day x-ray singles measurement was also made and the M x-ray region is shown in Fig. 4. The intensities of the $L\alpha$ peaks in the singles and coincidence runs agreed within 2% which indicated the coincidence efficiency was close to 100%. The α spectra in coincidence with L x rays and M x rays are shown in Fig. 5 for eight days of measurement.

1. L x rays

Figure 2 shows the photon radiation between 9.3 and 18.3 keV in coincidence with ^{210}Po α particles. Characteristic lead L x rays are observed as well as impurity x rays from ^{241}Am near the detector. The $L\alpha$ peak arises from L_{III} vacancy filling, the $L\beta$ peaks arise from all three subshells and the $L\gamma$ peaks arise from the L_{I} and L_{II} subshells. A spectroscopic diagram of the radiative transitions that comprise the characteristic lead L x rays is given in Fig. 6.

From the total number of coincidences in a given peak shown in Fig. 2 and the x-ray detector efficiency curve, the following two ratios were found:

$$\frac{P_{L\alpha}}{P_{L\beta}} = 1.14 \pm 0.06 \ , \qquad \frac{P_{L\alpha}}{P_{L\gamma}} = 5.18 \pm 0.26 \ .$$

In addition the ratio $P_{L\alpha}/P_{Ll} = 20.0 \pm 4.0$ was determined from the singles spectrum (not shown) because the number of Ll events was too low in the coincidence measurement. $P_{L\alpha}$, for example, is the probability per α particle of emitting an L x ray belonging to the $L\alpha$ peak. From the total number of events in a given peak, the efficiency curve and the α singles counting rate the following abundances were obtained: $P_{L\alpha} = (1.11 \pm 0.11) \times 10^{-4}$, $P_{L\beta} = (9.72 \pm 0.78) \times 10^{-5}$, $P_{L\gamma} = (2.15 \pm 0.32) \times 10^{-5}$, and $P_{Ll} = (1.11 \pm 0.22) \times 10^{-6}$. Accidental coincidences and scattered radiation were negligible.

The probabilities $P_{L\alpha}$, $P_{L\beta}, \ldots$, etc., can be written in terms of $P_{L_{\mathrm{I}}}$, $P_{L_{\mathrm{II}}}$, and $P_{L_{\mathrm{III}}}$ which are the probabilities per α particle of shake-off in the

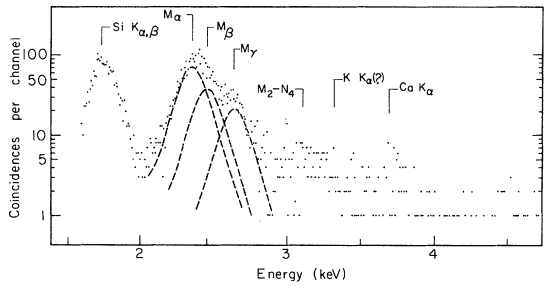

FIG. 3. Pb M x-ray spectrum (8.37 eV per channel) in coincidence with α particles.

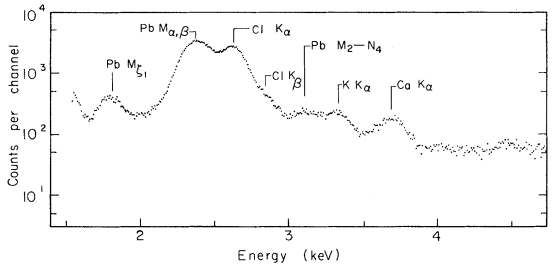

FIG. 4. M x-ray singles spectrum (8.37 eV per channel).

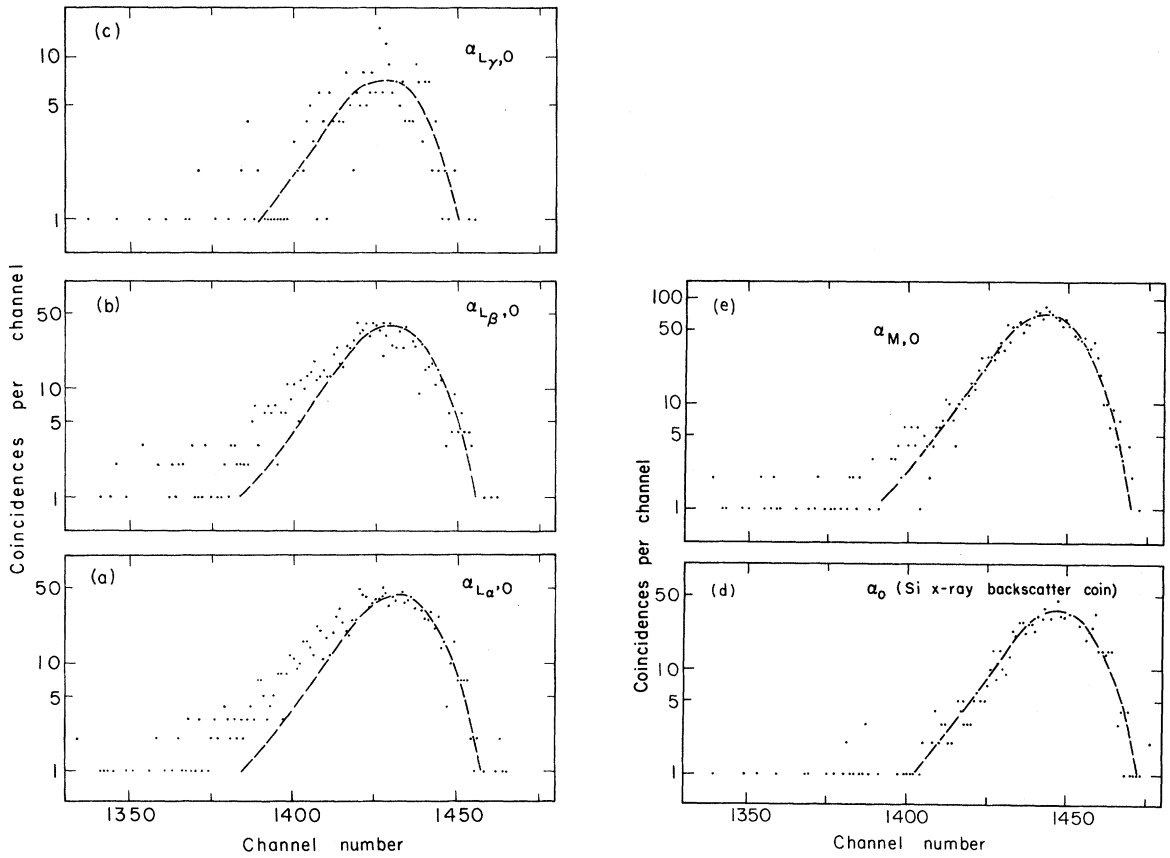

FIG. 5. (a)–(c) α spectrum (0.85 keV per channel) in coincidence with lead $L\alpha$, $L\beta$, and $L\gamma$ x rays. --- expected peak shape from calculated vacancy distribution and the assumption that the ejected electrons carry off zero kinetic energy. (d) α spectra (0.85 keV per channel) in coincidence with Si x rays. ---, smoothed peak shape. (e) α spectra (0.85 keV per channel) in coincidence with lead M x rays. ---, same peak shape as in (d) normalized to peak height.

$L_{\rm I}$, $L_{\rm II}$, and $L_{\rm III}$ subshells, respectively:

$$P_{L\alpha} = [P_{L_{\rm III}} + P_{L_{\rm II}} f_{23} + P_{L_{\rm I}}(f_{13} + f_{12} f_{23})]\,\omega_3 F_{3\alpha} \,, \tag{1}$$

$$P_{L\beta} = [P_{L_{\rm III}} + P_{L_{\rm II}} f_{23} + P_{L_{\rm I}}(f_{13} + f_{12} f_{23})]\,\omega_3 F_{3\beta} + (P_{L_{\rm II}} + P_{L_{\rm I}} f_{12})\omega_2 F_{2\beta} + P_{L_{\rm I}}\omega_1 F_{1\beta} \,, \tag{2}$$

$$P_{L\gamma} = (P_{L_{\rm II}} + P_{L_{\rm I}} f_{12})\omega_2 F_{2\gamma} + P_{L_{\rm I}}\omega_1 F_{1\gamma} \,, \tag{3}$$

$$P_{Ll} = [(P_{L_{\rm III}} + P_{L_{\rm II}} f_{23} + P_{L_{\rm I}}(f_{13} + f_{12} f_{23})]\,\omega_3 F_{3l} \,. \tag{4}$$

The experimental resolution of the L x rays was sufficient to resolve $L\gamma$ into $L\gamma_1$ and $L\gamma_c$ (see Fig. 6) and their probabilities can be expressed as:

$$P_{L\gamma_1} = (P_{L_{\rm I}} f_{12} + P_{L_{\rm II}})\omega_2 F_{2\gamma_1} \,, \tag{5}$$

$$P_{L\gamma_c} = (P_{L_{\rm I}} f_{12} + P_{L_{\rm II}})\omega_2 F_{2\gamma c} + P_{L_{\rm I}}\omega_1 F_{1\gamma_c} \,. \tag{6}$$

Also, we can write for $P_{L\beta_{1,2}}$ and $P_{L\beta_4}$

$$P_{L\beta_{1,2}} = [P_{L_{\rm III}} + P_{L_{\rm II}} f_{23} + P_{L_{\rm I}}(f_{13} + f_{12} f_{23})]\,\omega_3 F_{3\beta_2} + (P_{L_{\rm II}} + P_{L}\ f_{12})\omega_2 F_{2\beta_1} \,, \tag{7}$$

$$P_{L\beta_4} = P_{L_{\rm I}}\omega_1 F_{1\beta_4} \,, \tag{8}$$

where f_{12}, f_{13}, and f_{23} are the values of the Coster-Kronig (C-K) yields and ω_1, ω_2, and ω_3 are the values of the subshell fluorescence yields.[11] F_{ij} represent the fraction of radiative transitions in the L_j peak connected with filling a vacancy in the

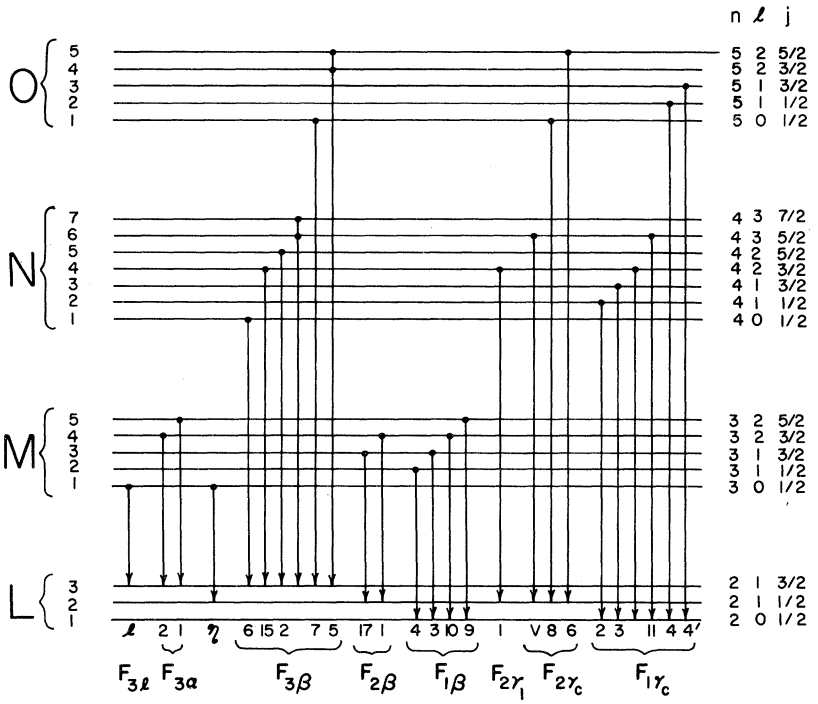

FIG. 6. Diagram of radiative transitions. Spectroscopic diagram for the major radiative transitions that comprise the characteristic L x ray spectrum.

L_i subshell. Thus, for example,

$$F_{1\beta}=\frac{\sum\Gamma_{1\beta}}{\Gamma_1}$$

$$=\frac{\text{intensity of } L_\beta \text{ x rays originating from } L_1 \text{ vacancies}}{\text{total intensity of x rays originating from } L_1 \text{ vacancies}}$$

$$=\frac{\Gamma(L\beta_4)+\Gamma(L\beta_3)+\Gamma(L\beta_{10})+\Gamma(L\beta_9)}{\Gamma_1}\ .$$

Two sets of radiative rates were used. One was the set calculated by Scofield,[12] and the other is an experimental set tabulated by Salem and Schultz.[13] Since Salem and Schultz listed only the major transitions (>90%) we normalized their total value to Scofield's for the same transitions. From the L x-ray singles spectrum measured in the present work, the ratio $F_{1\beta}/F_{1\gamma_{2,3}}$ agreed better with that determined from the Salem-Schultz list than Scofield's. We therefore believe the treatment using the former is the more accurate.

The probabilities P_{L_I}, $P_{L_{II}}$, and $P_{L_{III}}$ were calculated (see Table I) by two different methods. In method I Eqs. (5) and (6), which are linearly independent, are easily solved for P_{L_I} and $P_{L_{II}}$, and then $P_{L_{III}}$ is calculated from Eq. (1). In this method only the data obtained in the coincidence run are used. The errors are calculated by assuming a maximum uncertainty of 10% in resolving $L\gamma$ into $L\gamma_1$ and $L\gamma_c$ and do not include any errors in the C-K coefficients ω or F_{ij}. The consistency of the calculation is checked by determining $P_{L\beta}$ from Eq. (2), and the resulting value 0.99×10^{-4} agrees well with the experimental value 0.97×10^{-4}. In method II the values of $P_{L\beta_{1,2}}$ and $P_{L\beta_4}$ are obtained from the x-ray singles spectrum. Equation (8) is solved for P_{L_I}, and then Eqs. (7) and (1) are solved for $P_{L_{II}}$ and $P_{L_{III}}$. With an assumption of 5% uncertainty in the determination of the ratio $P_{L\beta_4}/P_{L\beta}$, errors were calculated in the same way as for method I. With these calculated possibilities the abundance of $P_{L\gamma}$ as determined from Eq. (3), 0.21×10^{-4}, agrees well with the experimental value 0.22×10^{-4}. The consistency of the calculations for both methods indicates that uncertainties in the F_{ij} values probably contribute

TABLE I. L Subshell electron shake-off probabilities.

Shells	Probabilities ($\times 10^4$) I[a]	II[b]	Errors[c]
P_{L_I}	4.92 ± 0.64	5.11 ± 0.40	1.70
$P_{L_{II}}$	0.73 ± 0.24	0.62 ± 0.06	0.46
$P_{L_{III}}$	1.60 ± 0.30	1.50 ± 0.19	0.84
P_L	7.25 ± 1.18	7.23 ± 0.65	0.91
P_{L_x}	2.39 ± 0.39	2.37 ± 0.21	

[a] Method I with Salem and Schultz's F_{ij}. (Possible errors in ω, f, and F_{ij} are not included.)
[b] Method II with Salem and Schultz's F_{ij}. (Possible errors in ω, f, and F_{ij} are not included.)
[c] Estimated uncertainties in fluorescence yields and Coster-Kronig coefficients are included (see Fig. 7).

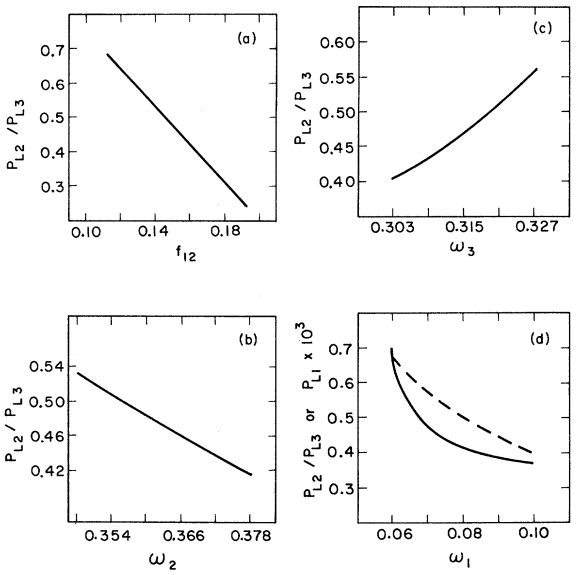

FIG. 7. Variation of deduced subshell probabilities as a function of input parameters. The values of ω and C-K are taken from Ref. 11 and are $\omega_1 = 0.08 \pm 0.02$, $\omega_2 = 0.363 \pm 0.015$, $\omega_3 = 0.315 \pm 0.013$, $f_{12} = 0.15 \pm 0.04$, $f_{13} = 0.57 \pm 0.03$, and $f_{23} = 0.164 \pm 0.016$. (a) $P_{L_{II}}/P_{L_{III}}$ vs f_{12}. (b) $P_{L_{II}}/P_{L_{III}}$ vs ω_2. (c) $P_{L_{II}}/P_{L_{III}}$ vs ω_3. (d) —, $P_{L_{II}}/P_{L_{III}}$ vs ω_1, ---, $P_{L_I} \times 10^3$ vs ω_1.

smaller errors to P_I, P_{II}, and P_{III} than our measurements contribute. The results obtained by the two different methods agree well with each other as shown in Table I, but method II gives more precise results and therefore the best values.

The total L-shell ionization probability per α particle $P_L = P_{L_I} + P_{L_{II}} + P_{L_{III}}$ is listed in Table I. Also listed in the total photon yield per α particle, P_{L_x}, which was determined from the equation:

$$P_{L_x} = P_{L_I}[\omega_1 + f_{12}\omega_2 + (f_{13} + f_{12}f_{23})\omega_3] + P_{L_{II}}(\omega_2 + f_{23}\omega_3) + P_{L_{III}}\omega_3 \ . \quad (9)$$

The sensitivity of the calculated subshell shake-off probabilities to the parameters ω and f was also considered. The variations in f_{13} and f_{23} within the published errors result in maximum changes of only 1 and 4%, respectively, in the ratio $P_{L_{II}}/P_{L_{III}}$. However, the possible variations in the other parameters result in much more pronounced changes as can be seen in Fig. 7. Variations in more than one parameter at a time could result in even larger changes than indicated. It is evident that more precise experimental or theoretical values of the input parameters are desirable.

2. *M x-rays*

Figure 3 shows the photon radiation between 1.4 and 4.7 keV in coincidence with ^{210}Po α particles. K and Si x rays, which were obtained by exciting KBr and Si sources with ^{55}Fe radiation, served as energy and peak calibration standards. Silicon K x rays excited in the α detector during the coincidence measurement were scattered into the x ray detector and these also served as an internal calibration. In the x-ray singles spectrum the α detector was masked by a nickel foil and Si x rays were not observed.

The M x-ray coincidence spectrum was resolved into its three major components: $M\alpha(M_V\text{-}N_{VI,VII})$, $M\beta(M_{IV}\text{-}N_{VI})$, and $M\gamma(M_{III}\text{-}N_V)$. The line $M_{III}\text{-}N_{IV}$ was also included in $M\gamma$. The abundances of the three components were determined as well as an upper limit on the number of counts registered in the $M_{II}\text{-}N_{IV}$ peak. After correcting for the x-ray detector efficiency the abundances of $M\alpha$, $M\beta$, $M\gamma$, and $M_{II}\text{-}N_{IV}$ x rays become $(2.9 \pm 0.6)\times 10^{-4}$, $(1.5 \pm 0.3)\times 10^{-4}$, $(0.8 \pm 0.16)\times 10^{-4}$, $< 0.18 \times 10^{-4}$, respectively. The ratios of the line intensities are $M\alpha : M\beta : M\gamma : M_{II}\text{-}N_{IV} = 100 : 52 : 27 : < 5$. These agree roughly with previous values[5] 100 : 66.6 : 33.3 : 10.

Figure 4 shows the corresponding M x-ray singles spectrum. Unfortunately, as was established after the experimental work was completed, intense chlorine K x-ray peaks masked part of the lead M x-ray energy region. X-ray fluorescence analyses of the same kind of beryllium foil as used for the ^{210}Po source backing plate showed large amounts of the Cl x-ray peaks. The chlorine possibly arises from trichlorethane which is used sometimes to rinse beryllium after it is machined. A low energy x-ray spectrum of ^{241}Am deposited on the same type of foil showed that the Cl x rays were roughly proportional to the α activity of the

source and indicated that less than 1% of the $M\gamma$ peak observed in the ^{210}Po coincidence experiment was due to Cl x rays. The $M\zeta_1(M_V\text{-}N_V)$ peak, which was masked by Si x rays in the coincidence experiments, is not affected in the singles measurement because of the Ni shield in front of the α detector. Its abundance is $(0.23\pm0.05)\times10^{-4}$ and the ratio $M\alpha:M\zeta_1$, is 100:8. This ratio agrees roughly with that deduced from the calculated[14] radiative transition probabilities, 100:3.5 but is in considerable disagreement with the ratio[5] 100:55.

From the coincidence counting rate, the average x-ray detector efficiency in the M x-ray region and the α singles counting rate, the photon yield per α particle P_{M_x} was calculated to be $(5.52\pm1.10)\times10^{-4}$. With an average fluorescence yield $\bar{\omega}_M=0.03$, the total M-shell ionization probability per α particle is $P_M=(1.84\pm0.37)\times10^{-2}$ excluding the uncertainty in the average fluorescence yield.

The large error associated with the above results is mostly due to the large uncertainty (10%) involved with the intensity of Np x rays that were used in the efficiency calibration of the x-ray detector.

Similar equations to the ones written for L x rays above can be written for the M x rays. But, the experimental data will not suffice to obtain unique results for the subshell ionization probabilities. However, from this type of analysis it is possible to determine several limits on the ionization probabilities, e.g. $P_{M_{II}}=7\text{–}23\%$, $P_{M_{IV}}<24\%$, $P_{M_V}<17\%$; $P_{M_V}+P_{M_{II}}f_{25}<17\%$, $P_{M_{IV}}+P_{M_{II}}f_{24}<28\%$, and $P_{M_I}+P_{M_{III}}>47\%$ of the total. The input parameters used were taken from Refs. 11 and 14 and an error of 10% was assumed in their values and in the relative values of the intensities of the M x-ray peaks.

3. α particles

Figures 5(a)–5(e) show α spectra of ^{210}Po which are in coincidence with various x rays. These spectra were obtained from data taken during eight days of the measurements in which the gain stabilizer on the α side maintained a constant peak amplitude. The peak in Fig. 5(d) is due to the main α_0 peak of ^{210}Po which excited Si x rays in the α detector, and these backscattered into the x-ray detector. This peak established the channel position of ^{210}Po α_0 and served as the peak-shape standard. In Figs. 5(a)–5(c) are shown α spectra in coincidence with Pb $L\alpha$, $L\beta$, and $L\gamma$ x rays, respectively. In Fig. 5(e) is shown the α spectra in coincidence with M x rays comprising $M\alpha$, $M\beta$, and $M\gamma$. The same type of nomenclature is used for labeling the peaks as suggested in an earlier paper.[1] ^{210}Po $\alpha_{L\alpha,0}$ for example, refers to the ground state α decay of ^{210}Po which shakes off an L electron resulting in an $L\alpha$ x ray.

In Figs. 5(a)–5(c) are also shown the peak shapes expected from the initial vacancy distributions given in Table I (last column) and the assumption that the ejected electrons carry off zero kinetic energy. In Fig. 5(e) the dashed line is the same curve as the peak shape standard shown in Fig. 5(d).

As mentioned earlier accidental coincidences were insignificant. The α peaks in coincidence with the $L\alpha$, $L\beta$, and $L\gamma$ x rays were, respectively, 12.6 ± 1.4, 13.8 ± 1.4, and 17.6 ± 2.1 keV lower in energy than α_0. These were in good agreement with the expected values determined from the binding energies of 13.035, 15.200, and 15.861 keV for the L_{III}, L_{II}, and L_I electrons, respectively. The peak due to M x rays is located 3.1 ± 1.0 keV lower than α_0 which is in good agreement with the M binding energies of 2.5 to 3.9 keV. The peaks due to L vacancies are broader than the one due to M vacancies which in turn is very slightly broader than the standard α peak.

III. DISCUSSION AND SUGGESTIONS

The shake-off phenomenon was explained by Migdal[15] as due to the slowly moving α particle adiabatically perturbing the atomic electron cloud. The probability of ejecting an electron was then given by a series expansion. Migdal calculated only the first term (dipole term) for the K, L, and M electrons (Migdal: formula 21). Levinger[16] used the same perturbation technique but included in the dipole term the contribution of the recoiling nucleus to the perturbing potential. He neglected the recoil effect in the quadrupole term since its contribution to that term was very small and recalculated the shake-off probabilities only for K and L electrons (Levinger: Table IV corrected as noted by author). The inclusion of the recoiling nucleus in the perturbing potential is considered questionable,[17,18] and after the recoil contribution is factored out, Levinger's calculations of the dipole term are identical to Migdal's.

In Table II we summarized the experimental work on L and M electron shake-off accompanying α decay and compared it with theoretical predictions. For the effective charges the following values were used:

$$Z^*_{2s}=77.34,\quad Z^*_{2p}=76.23\ ,$$

$$Z^*_{3s}=69.28,\quad Z^*_{3p}=67.33\ ,\quad Z^*_{3d}=64.81\ .$$

The L-subshells ionization probabilities are all

TABLE II. Probability of electron shake-off from the L and M shells. D denotes dipole term, and Q denotes quadrupole term.

Shell		Theory: Migdal (Ref. 15)	Theory: Hansen (Ref. 18)	Experiment [a]	Ref.
	D	4.300×10^{-5}			
	Q	0.002×10^{-5}			
P_{L_I}	Total	4.302×10^{-5}	2.30×10^{-4}	$(5.11\pm0.40)\times10^{-4}$	This work
	D	2.791×10^{-5}			
	Q	0.889×10^{-5}			
$P_{L_{II}}$	Total	3.680×10^{-5}	0.76×10^{-4}	$(0.62\pm0.06)\times10^{-4}$	This work
	D	5.582×10^{-5}			
	Q	2.525×10^{-5}			
$P_{L_{III}}$	Total	8.107×10^{-5}	2.86×10^{-4}	$(1.50\pm0.19)\times10^{-4}$	This work
P_L		1.61×10^{-4}	5.9×10^{-4}	$(7.23\pm0.65)\times10^{-4}$	This work
P_{L_x}		0.54×10^{-4}	1.83×10^{-4}	$(2.2\pm0.5)\times10^{-4}$	3
				$(2.93\pm0.43)\times10^{-4}$	4
				$(2.79\pm0.42)\times10^{-4}$	5
				4×10^{-4}	2
				$(2.37\pm0.21)\times10^{-4}$	This work
P_M		1.67×10^{-3}	1.90×10^{-2}	$(1.84\pm0.37)\times10^{-2}$ [b]	This work
P_{M_x}		5.01×10^{-5}	5.7×10^{-4}	$(5.5\pm1.1)\times10^{-4}$	This work
				1.5×10^{-3}	2
				0.91×10^{-3}	5

[a] The errors in this table do not include uncertainties in the values of ω, f, and F_{ij}. (The effect of most of these uncertainties is shown in Table I and Fig. 7.)

[b] Uncertainties in ω and C-K coefficients would increase the given error to $\pm0.6\times10^{-2}$.

smaller than the probabilities from the experiment and the theoretical series expansion converges rather slowly. These suggest the need to calculate additional terms in the series expansion. Also, a more realistic set of wave functions relativistic Hartree-Fock wave functions, for example, should be used in the calculation rather than the hydrogenic type. Similar remarks can be made with regard to M-shell shake-off calculations.

Recently, in a different type of theoretical treatment Hansen[18] calculated the shake-off probabilities of K, L, and M electrons. In his treatment, each of the above probabilities were described as a special zero-impact-parameter trajectory in the generalized impact-parameter formulation of a binary encounter approximation. His results are in good agreement with the total experimental photon yield (L and M) per α particle. However, the agreement is not as good for the individual L-subshell ionization probabilities. It will be interesting to compare the differential shapes of the α spectra with those from Hansen's treatment when the latter becomes available.

IV. OTHER VERY RECENT WORK ON ^{210}Po

Scott[19] published a paper on the abundances of $L\alpha$ rays in ^{210}Po decay. In general his abundances were about 60% of our values and are considerably lower than those of other workers. His abundances ($\times10^4$) for Ll, $L\alpha$, $L\beta$, and $L\gamma$ were 0.044 ± 0.01, 0.68 ± 0.05, 0.58 ± 0.05, and 0.11 ± 0.01. These compare with our values of 0.0111 ± 0.0022, 1.11 ± 0.11, 0.972 ± 0.078, and 0.215 ± 0.032.

Unpublished work by Fischbeck and Freedman[20] give a total value for $P_L\times10^4$ of 8.2 ± 0.5 vacancies and a weighted average of all work excluding ours and Scott's of 8.1 ± 0.5. This compares with our value of 7.23 ± 0.62. These authors also studied the electron and α distribution as a function of energy.

Briand *et al.*[21] found a value of 3.2 ± 0.8 for $P_{LX}\times10^{-4}$ which compares with our value of 2.37 ± 0.21.

ACKNOWLEDGMENTS

We greatly appreciate the considerable help of Duane Mosier of the Lawrence Berkeley Laboratory for many consultations and detailed suggestions on the type of equipment used in the experiments and the use of the program MULTI to reduce the data. We also are indebted to Robert D. Giauque and Dr. Alvin J. Hebert for their x-ray fluorescence measurements.

*Work performed under the auspices of the U. S. Atomic Energy Commission.

†Present address: The Hebrew University, Jerusalem, Israel.

[1]M. S. Rapaport, F. Asaro, and I. Perlman, preceding paper, Phys. Rev. C 11, 1740 (1975).

[2]I. Curie and F. Joliot, J. Phys. (Paris) 7, 20 (1931).

[3]M. Riou, J. Phys. (Paris) 13, 487 (1952).

[4]W. Rubinson and W. Bernstein, Phys. Rev. 86, 545 (1952).

[5]W. Rubinson, Phys. Rev. 130, 2011 (1963).

[6]J. S. Hansen, J. C. McGeorge, D. Nix, W. D. Schmidt-Ott, I. Unus, and R. W. Fink, Nucl. Instrum. Methods 106, 365 (1973).

[7]J. Legrand, Nucl. Instrum. Methods 112, 229 (1973).

[8]J. L. Campbell and L. A. McNelles, Nucl. Instrum. Methods 98, 433 (1972).

[9]D. A. Landis, C. F. Jones, B. V. Jarrett, A. Jue, and S. D. Wright, LBL Report No. LBL-540, 1972 (unpublished).

[10]D. F. Mosier, Lawrence Berkeley Laboratory (unpublished).

[11]W. Bambynek, B. Crasemann, R. W. Fink, H. U. Freund, H. Mark, C. D. Swift, R. E. Price, and P. V. Rao, Rev. Mod. Phys. 44, 716 (1972).

[12]J. H. Scofield, Phys. Rev. 179, 9 (1969).

[13]S. I. Salem and C. W. Schultz, At. Data 3, 215 (1971).

[14]C. P. Bhalla, J. Phys. B 3, 916 (1970).

[15]A. Migdal, J. Phys. (USSR) 4, 423 (1941).

[16]J. S. Levinger, Phys. Rev. 90, 11 (1953); J. Phys. (Paris) 16, 556 (1955).

[17]V. V. Ovechkin and E. M. Tsenter, At. Energ. 2, 282 (1957) [Sov. J. At. Energy 2, 344 (1957)].

[18]J. S. Hansen, Phys. Rev. A 9, 40 (1974).

[19]R. D. Scott, J. Phys. A 7, 1171 (1974).

[20]H. J. Fischbeck and M. S. Freedman, Phys. Rev. Lett. 34, 173 (1975).

[21]J. P. Briand, P. Chevallier, A. Johnson, J. P. Rozet, M. Tavernier, and A. Touati, Phys. Rev. Lett. 33, 266 (1974).